Influence of alloying elements and microstructure on aluminium sacrificial anode performance: case of Al–Zn

D.R. SALINAS*, S.G. GARCÍA and J.B. BESSONE
Inst. de Ing. Electroquímica y Corrosión (INIEC), Dpto. de Qca. e Ing. Qca., Universidad Nacional del Sur, 8000 Bahía Blanca, Argentina
(*author for correspondence, e-mail: dsalinas@criba.edu.ar)

Abstract

The electrochemical behaviour of Al–x%Zn alloys (1 wt % $\leqslant x \leqslant$ 80 wt %) was studied in 0.5 M sodium chloride solution. The experiments focused on the influence of casting conditions on sacrificial anode performance. The influence of casting conditions, solidification structure, polarization behaviour and attack morphology on the anode efficiency and operating potential was analysed. For alloys with low Zn content (1–5 wt %), the interdendritic zones or grain boundaries were the initial sites of attack and self corrosion was the principal cause of efficiency loss. Particularly, for Zn contents below 3 wt % the operating potential was strongly affected by the solidification macrostructure. Casting conditions that produced better alloying element distribution (chill structures) promoted higher anode efficiency. For Zn content higher than 5 wt % the operating potential and the anode efficiency were defined by the α/β phases area relationship.

1. Introduction

The performance of aluminium sacrificial anodes is directly related to the electrochemistry of alloys. In practice, the majority of metallic surfaces cannot be considered of ideal homogeneity as a whole. In contrast, compositional and structural variations are expected and it is better to consider that different phases are present as solid solution or segregates. The solidification structure is a function of the initial nominal composition and the heat extraction rate. When an ingot is frozen, three separate phases of the freezing process may occur, with each phase developing a characteristic arrangement of crystal sizes and shapes. In a narrow band following the contour of the mold lies the 'chill zone', consisting of small equiaxed (equal-sized) crystals, which usually have random orientations. Inside of this outer zone the crystals become larger in size, elongated in shape, with their lengths parallel to the heat-flow direction (normal to the mold walls). Because of the shape of the crystals in this zone, it is customary to call it the 'columnar zone'. The last zone lies at the centre of the ingot and represents the last metal to freeze. In this region the grains are again equiaxed and of random orientation. Accordingly, planar, cellular or dendritic grain growth will take place [1], where chill, columnar or equiaxial grains are favoured. Consistently, the alloying element distribution, either in solid solution or as segregated second-phase particles, intermetallic compounds or inclusions, depend on the casting conditions used. In the case of aluminium-based sacrificial anodes, the operating potential and efficiency are expected to be directly related to these metallurgical features.

Since 1966 [2], ternary aluminium-based alloys, such as Al–Zn–In or Al–Zn–Sn have been used as sacrificial anodes. Nevertheless, several aspects related to the performance of these alloys remain uncorrelated; namely, the relation between the solidification rate and alloying element distribution with the anode efficiency. Previous studies [3] showed strong effects produced by different cooling conditions in Al–Zn–Sn alloys. The attack initiation and propagation strongly depend on local zones, where an enrichment of the alloying elements occurs. Also, the coexistence of different metallurgical structures (chill, columnar or equiaxial) operates detrimentally to anode efficiency. This effect was present in experiments carried out on Al–5 wt % Zn–0.1 wt %Sn galvanic anodes operated in sea water for 200 days [4]. In this case the macroattack morphology presented an external layer with 'metallic sponge' characteristics, followed by an intermediate zone with slight dissolution and a central one with pronounced pitting. These features were promoted by an accentuated macrosegregation which induced changes in the electrochemical behaviour during the operation time. Theoretically, uniform anode dissolution will give maximum efficiency [5]. Either secondary cathodic reaction on the same interface and/or mechanical grain loss due to local

Table 1. Content of impurities in aluminium and zinc

	Composition/wt %											
	Fe	Si	Cu	Ti	V	Ga	Mg	Ni	Pb	Sn	Zn	Al
Al 99.9 (Al$_p$)	0.01	0.05	0.001	0.0014	0.0011	0.009	0.001	0.001	–	–	0.002	Bal.
Al 99.8 (Al$_c$)	0.10	0.07	0.004	0.0029	0.0018	0.008	0.002	0.001	–	–	0.005	Bal.
Zn 99.9	0.02	–	0.001	–	–	–	–	–	0.005	0.001	Bal.	–

macro- or microcorrosion cells will reduce the anode efficiency.

In practice, all Al sacrificial anodes are based on the binary Al–Zn system [5, 6]. In Al–Zn alloys, Zn tends to be rejected to interdendritic zones or grain boundaries [3]. This effect is favoured by the cooling rate and the alloying element characteristics (lower melting point than aluminium). Under polarization, this local composition variation will favour the initiation and propagation of macro- and micro-local events (i.e., galvanic corrosion or pitting). These events are responsible for lowering the anode efficiency either by electrochemical or mechanical mass loss (grain or particles drop).

The experiments in this paper are focused on the influence of possible casting conditions on the operational performance of the Al–x%Zn system, which is the base alloy for all industrial aluminium sacrificial anodes.

2. Experimental details

Tests specimens were Al–1 wt %Zn, Al–3 wt %Zn, Al–5 wt %Zn, Al–20 wt %Zn, Al–40 wt %Zn, Al–60 wt %Zn and Al–80 wt %Zn. All were obtained from zinc (99.9%) and two types of unalloyed aluminium ('pure', Al 99.9%; commercial, Al 99.8%), with nominal composition shown in Table 1. Unless otherwise stated, the Al–Zn alloys were obtained from 'pure' Al. The alloys were cast in an iron mold (height, $h = 100$ mm, diameter, $d = 24$ mm) and both melted mass and mold temperatures were controlled according to Table 2. In all cases the aim was to obtain only one type of metallurgical structure (chill, columnar or equiaxial), avoiding superposition effects. For comparative purposes, unalloyed aluminium ingots were also cast with the mentioned structures. Cylindrical anodes (20 mm high × 20 mm dia.) were machined from the ingots, eliminating the structure formed by direct contact with the mold wall. The cylindrical wall of these samples was covered with cured epoxy resin, leaving only their cross section area of 2.8 cm^2 exposed. Thus, the different solidification zones were tested. All the specimens were polished with 1200 emery paper, then degreased in acetone, washed thoroughly in double-distilled water and kept in a desiccator.

An accelerated dissolution test (galvanostatic, $i = 1$ mA cm^{-2}, 30 days) was carried out to determine efficiencies and working potentials. All potentials were measured relative to a saturated calomel reference electrode (SCE). The solution used was 0.5 M NaCl, pH 5, prepared with chemicals of analytical grade and distilled water. Several electrochemical cells of 500 mL each with steel cathodes, connected in parallel, were used. The electrolyte total volume was 100 dm^3 and was recirculated automatically after 6 h, and totally changed after 24 h. At the end of the test the samples were removed, cleaned and weighed to obtain a weight loss. The total anode efficiency was calculated by knowing the total charge passed through the system, the weight loss of the anode specimen and the corresponding electrochemical equivalent. Cathodic impurities cause local cell action which leads to a decrease in anode efficiency, and hydrogen evolution is the primary cathodic reaction taking place at these local cells. Thus, the amount of hydrogen gas evolved from the anode is a measure of the amount of unwanted local cell reactions. Consequently, the efficiency loss by hydrogen evolution was calculated by measuring the volume of gas collected during the operation time, the time of collection and the current flow throughout the test. Finally, the mechanical loss of efficiency was calculated by difference between the total anode efficiency loss and the loss of efficiency by the hydrogen reaction. This mechanical loss of efficiency is caused by a selective attack on some phases, leaving behind a matrix of unreacted metal which may fall off in pieces. After the accelerated dissolution test

Table 2. Anodes casting conditions

Nominal composition	T_{liq} /°C	T_{mold} /°C	Cooling rates /kW cm^{-2}	Macrostructural aspect
Unalloyed Al	700	700	(a)	equiaxial
	700	0	0.446	columnar
	665	–10	0.667	chill
Al–1%Zn	705	705	(a)	equiaxial
	700	0	0.446	columnar
	670	–10	0.663	chill
Al–3%Zn	705	705	(a)	equiaxial
	750	0	0.407	columnar
	673	–10	0.658	chill
Al–5%Zn	715	715	(a)	equiaxial
	780	0	0.385	columnar
	680	–10	0.656	chill
Al–20,40,60,80%Zn	715	715	(a)	equiaxial

(a) in furnace (200° h^{-1})

the corroded surfaces were examined by optical or electronic microscopy to correlate the dissolution features with the microstructure.

For the assessment of current efficiency, as well as attack morphology, each corroded sample was chemically cleaned in a mixture of 2% chromic acid and 5% phosphoric acid at 80 °C for 4 min, rinsed with double-distilled water, dried at room temperature and finally weighed.

The solidification structure and the segregates distribution were revealed by means of Keller reagent [7]. With this etching reagent different constituents or parts of the metal are attacked selectively and reveal themselves as a pattern. They were observed by optical and scanning electron microscopy equipped with EDX analysis and characterized by X-ray diffraction analysis.

3. Results and discussion

The Al–Zn binary-phase equilibrium diagram is relatively simple [8, 9] (Figure 1) and shows mainly two solid solutions α and β, where the α range also embraces α'. Zinc as solute, presents an equilibrium partition ratio [1] $K < 1$. In between the two single phase alloys, a wide composition range is given by alloys with two phases ($\alpha + \beta$). Under nonequilibrium casting conditions, a mixture of these phases is expected at room temperature. For low Zn content in the alloy ($\leqslant 5$ wt %Zn) an α single phase prevails and for higher Zn content (>5 wt %) the β phase is also present.

3.1. Low Zn content range ($\leqslant 5$ wt %)

Following the casting conditions presented in Table 2, unalloyed commercial aluminium (Al$_c$) anodes and Al–Zn anodes with chill, columnar or equiaxial structures were obtained (Figure 2). An accelerated galvanostatic dissolution test at 1 mA cm^{-2} in 0.5 M NaCl was
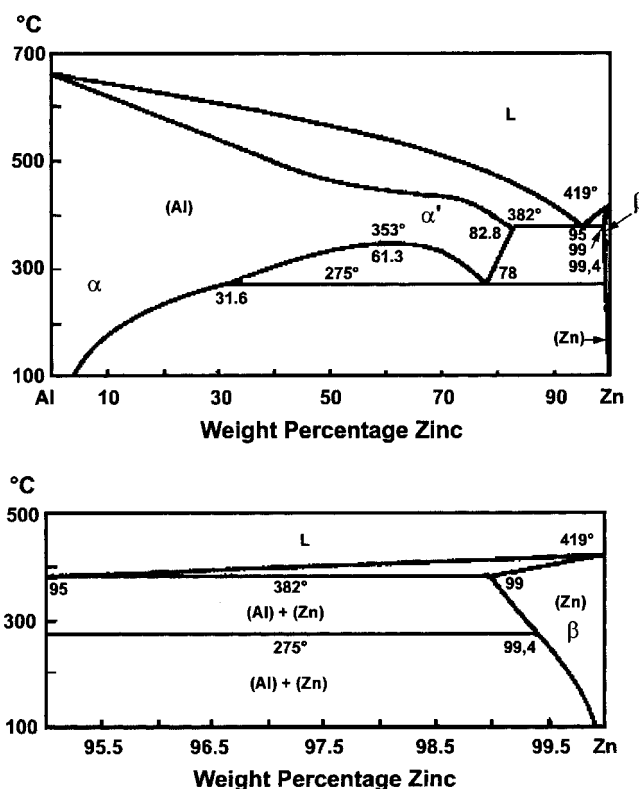
Fig. 1. Binary-phase diagram for Al–Zn system.

performed on these anodes over 30 days and the results are shown in Table 3. The total efficiency given by commercial aluminium is over 82% and practically equal for each type of structure studied. Nevertheless, the alloys show very low efficiencies and it is clearly observed that the main efficiency loss is owing to the secondary reaction. This result is produced by the relatively high content of impurities, particularly Fe and Cu, that cause local cell action [10, 11]. At low zinc content the dependence of the operating potential E_{op} on the solidification structure is relatively significant, with different values for each structure. As the zinc
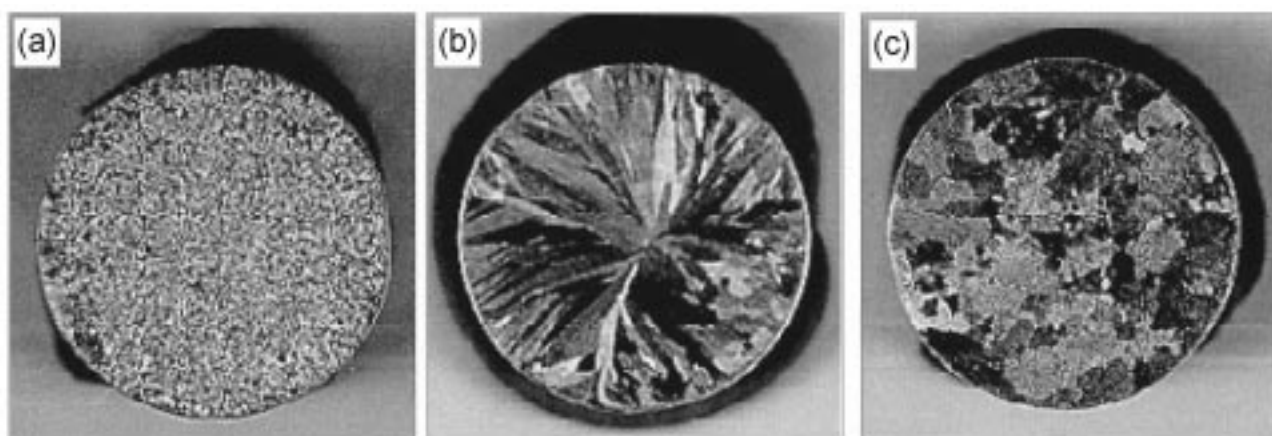
Fig. 2. Macroscopic transverse views of the anodes showing the metallurgical structures analysed. (a) Chill structure; (b) columnar structure; (c) equiaxial structure.

Table 3. Operating potential (E_{op}) and efficiencies of the binary Al–Zn alloys studied, after 30 day operation ($i = 1$ mA cm^{-2})

Alloy		E_{op} /mV	Efficiencies/%		
			Total efficiency	Efficiency loss by H$_2$ evolution	Efficiency loss by fall out of grains
Al$_c$	Chill	−720	82	12	6
	Columnar	−720	82	13	5
	Equiaxial	−720	83	13	4
Al$_c$–1%Zn	Chill	−863	48	45	7
	Columnar	−853	69	30	1
	Equiaxial	−825	40	52	8
Al$_c$–3%Zn	Chill	−933	27	60	13
	Columnar	−932	46	50	4
	Equiaxial	−935	48	48	4
Al$_c$–5%Zn	Chill	−955	40	56	4
	Columnar	−956	60	37	3
	Equiaxial	−955	68	23	9

Table 4. Operating potential (E_{op}) and efficiencies of the binary Al–Zn alloys studied, after 30 day operation ($i = 1$ mA cm^{-2})

Alloy		E_{op} /mV	Efficiencies/%		
			Total efficiency	Efficiency loss by H$_2$ evolution	Efficiency loss by fall out of grains
Al$_p$–1%Zn	Chill	−880/−900	80	15.8	4.2
	Columnar	−874/−882	82	12.5	5.5
	Equiaxial	−860/−880	82.3	13.5	4.2
Al$_p$–5%Zn	Chill	−965	80	10.7	9.3
	Columnar	−965	81	9.9	9.1
	Equiaxial	−965	81.4	9.2	9.4

content increases, this dependence tends to disappear and the operating potentials reach the well-known value $E_{op} = -960$ mV for 4–5 wt %Zn [4]. More negative E_{op} values favour the hydrogen reaction and the efficiency loss by the secondary reaction is increased in relation to unalloyed aluminium.

Table 4 shows the performance of Al$_p$–1 wt %Zn and Al$_p$–5 wt %Zn anodes with pure Al quality (Al$_p$). Clearly, the loss of efficiency by the secondary reaction is drastically reduced and the total efficiency is about 80%. Al$_p$–3 wt %Zn alloys showed similar trends. The tendency in the E_{op} values is practically the same as recorded in Table 3, showing erratic values for Al$_p$–1 wt %Zn alloys and a well defined $E_{op} = -965$ mV for Al$_p$–5 wt %Zn.

Considering the Al–1 wt %Zn alloy type analysed (Tables 3 and 4) the chill structure have the more negative E_{op} values and the alloys with equiaxial structure the more positive ones.

Although the efficiency loss by the hydrogen reaction masks the possible influence of the solidification structure on the efficiencies, some information can be obtained from the corrosion patterns observed on the anodes after the test. Figures 3 and 4 show the attack morphology developed on Al$_p$–1 wt %Zn and Al$_p$–5 wt %Zn alloys respectively. For Al$_p$–1 wt %Zn with chill and equiaxial structures, a localized, maldistributed intergranular and interdendritic attack is observed. These attack morphologies are possible due to the segregation of the poor zinc content and the impurities to those zones. This segregation is promoted by the solidification process. Probably, in each case the magnitude of the active areas is different and this situation would be the reason for the different operational potentials noted. These facts suggest that in the long term, heavy grain drop will occur and the mechanical loss of efficiency will increase drastically. Conversely, for Al$_p$–5 wt %Zn a higher Zn content promotes a better alloying element distribution, and consequently a more uniform attack. Although higher mechanical loss has appeared in this case, it should remain constant for the rest of its life.

In alloys with columnar structure, a concentric band attack is observed (Figures 3(b) and 4(b)). This partic-
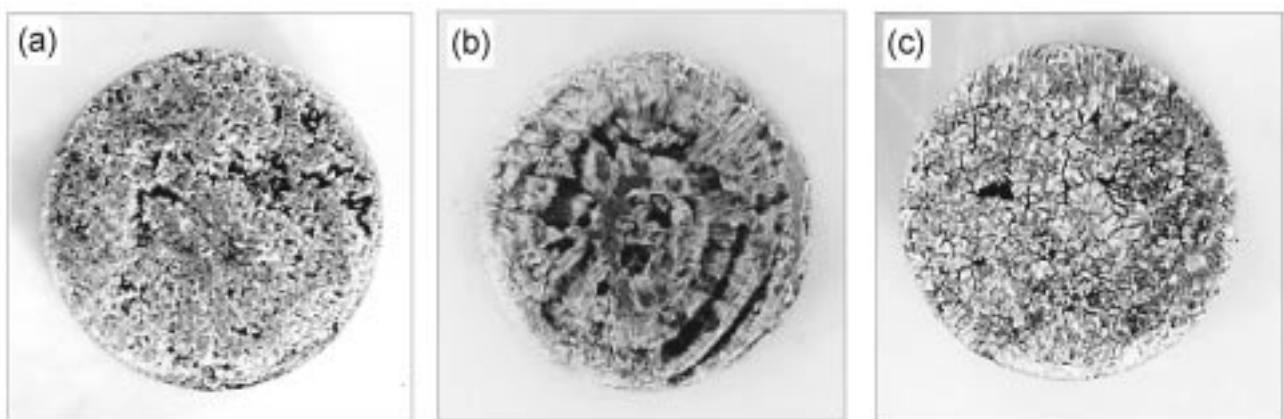

Fig. 3. Macroscopic views of the Al$_p$–1 wt %Zn anodes after the accelerated galvanostatic dissolution test (30 days, $i = 1$ mA cm^{-2}) in 0.5 M NaCl solution, pH 5. (a) Chill structure; (b) columnar structure; (c) equiaxial structure.
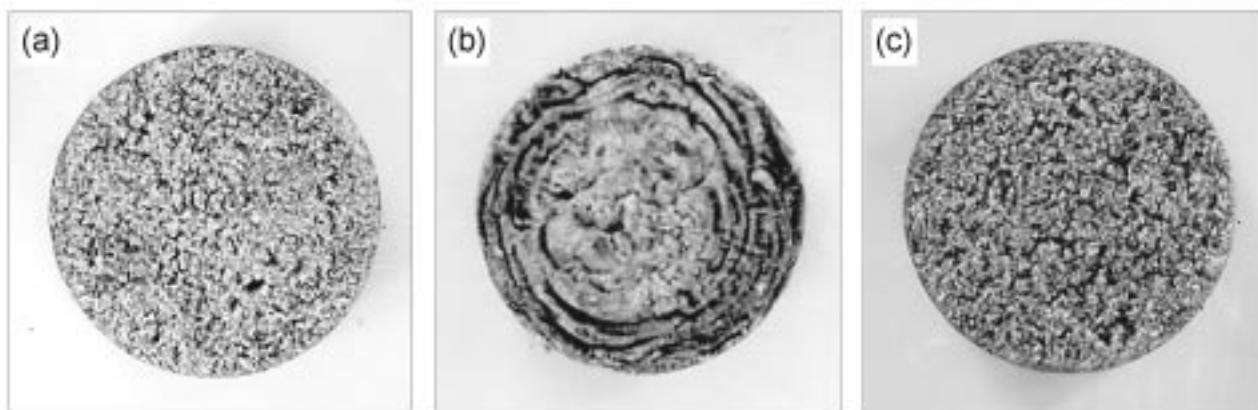
Fig. 4. Macroscopic views of the Al_p–5 wt %Zn anodes after the accelerated galvanostatic dissolution test (30 days, $i = 1$ mA cm^{-2}) in 0.5 M NaCl solution, pH 5. (a) Chill structure; (b) columnar structure; (c) equiaxial structure.

ular feature also appeared in previous studies on Al–5 wt %Zn–0.1 wt %Sn [4]. A cross sectional view of the corroded area (Figure 5(a)) shows a localized deep attack. An EDX line profile analysis produced just in front of the tip (Figure 5(b)), denotes Zn enrichment. This banding effect given by the solute concentration distribution is a result of either fluctuations in the solidification rate or in the thickness of the diffusion boundary layer during the crystal growth [1]. The significant amount of Zn concentrated in these radial bands facilitates a severe macroattack localization producing a detrimental anode operation. As the anode is consumed, zones with different alloying element concentrations are exposed, which lead to variations with time in the E_{op} values and nonuniform anode dissolution. This macrosegregation process is observed in all the studied alloys with columnar structure, irrespective of the Zn composition. Therefore, columnar structure should be avoided in anodes to eliminate this macrosegregation effect. In the following discussion only anodes with chill or equiaxial structure will be considered.

Galvanostatic polarization was applied on each anode after the 30 day test (Figure 6). Under these conditions, the actual active electrode area has already reached a steady state value, where no further pitting propagation process operates. As already known [12], as the Zn content increases the activation potential shifts to more negative values. The polarization behaviour of the alloys is practically independent of the metallurgical structure for Zn content higher than 3 wt %. According to Table 4, the Al–1 wt %Zn alloy with chill structure operates at more negative potential values than the Al–1 wt %Zn equiaxial, in all the current density range considered. This means that the anode efficiency obtained at low current densities will be the same as that obtained at high current densities. Therefore, these results consolidate the accelerated dissolution test performed.

X-Ray diffraction analyses were applied to characterize the phases present in the alloys. The X-ray diffraction diagrams of the different Al–Zn alloys, as well as those of pure Zn and Al, are given in Figure 7(a). In the
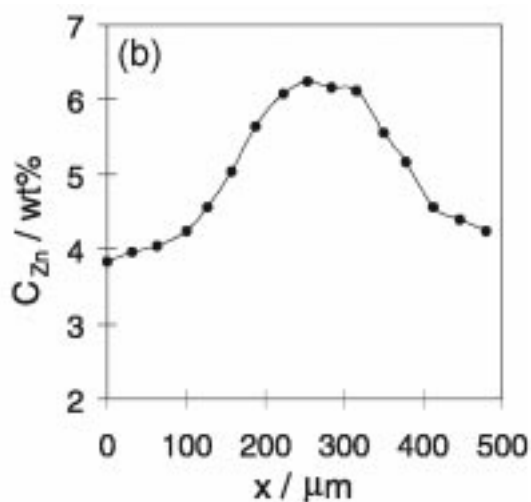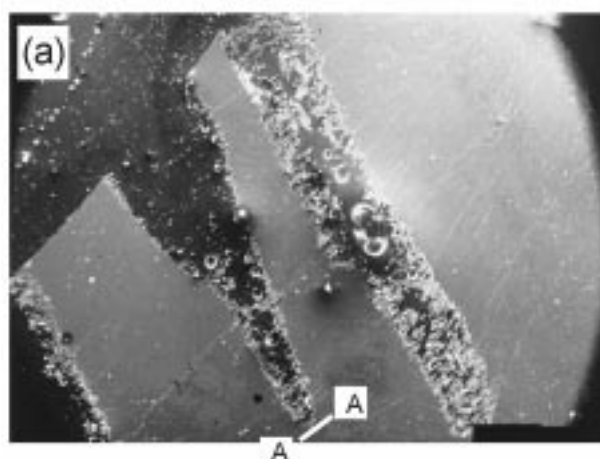

Fig. 5. (a) SEM micrograph showing the attack morphology developed on alloys with columnar structure (Al_p–1 wt %Zn case); (b) EDX line profile result obtained on A–A line.
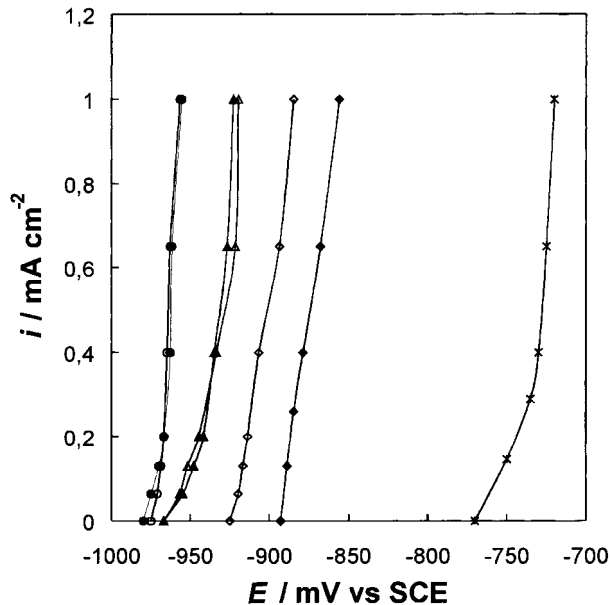
Fig. 6. Galvanostatic polarization curves of Al$_p$–Zn alloys with low Zn content (1–5 wt %) after the accelerated dissolution test. Solution: 0.5 M NaCl, pH 5. Legend: (○) Al–Zn 5% (chill); (●) Al–Zn 5% (equi.); (△) Al–Zn 3% (chill); (▲) Al–Zn 3% (equi); (◇) Al–Zn 1% (chill); (◆) Al–Zn 1% (equi.); (×) unalloyed Al.

alloys no peaks inherent to the Zn pattern appeared. This indicates that a β phase is not detected and only the α phase is formed (Figure 1). Figure 7(b) shows the diffraction patterns obtained at relatively high diffraction angles 2θ. As the Zn content increases from 1 to 5 wt % a decreasing peak intensity is recorded. At the same time the peaks are slightly shifted towards lower angles, denoting an increase in the lattice parameter (Table 5). These results suggest the incorporation of Zn in the structure of the α phase.

From the previous results it is possible to conclude that in the presence of cathodic impurities such as Cu, Fe and Si, the main efficiency loss is due to the secondary reaction. When the impurity content is lowered the metallurgical structure will have greater influence on the anode efficiency, specially for Zn content below 3 wt %. In this situation the anode performance depends on the alloying element segregated towards the grain boundaries and interdendritic zones, and this process is strongly affected by the casting conditions. This is the case with the Al–1 wt %Zn alloy with chill structure. In alloys with this structure, the alloying elements are concentrated at the grain boundaries due to the segregation process [3], promoting a
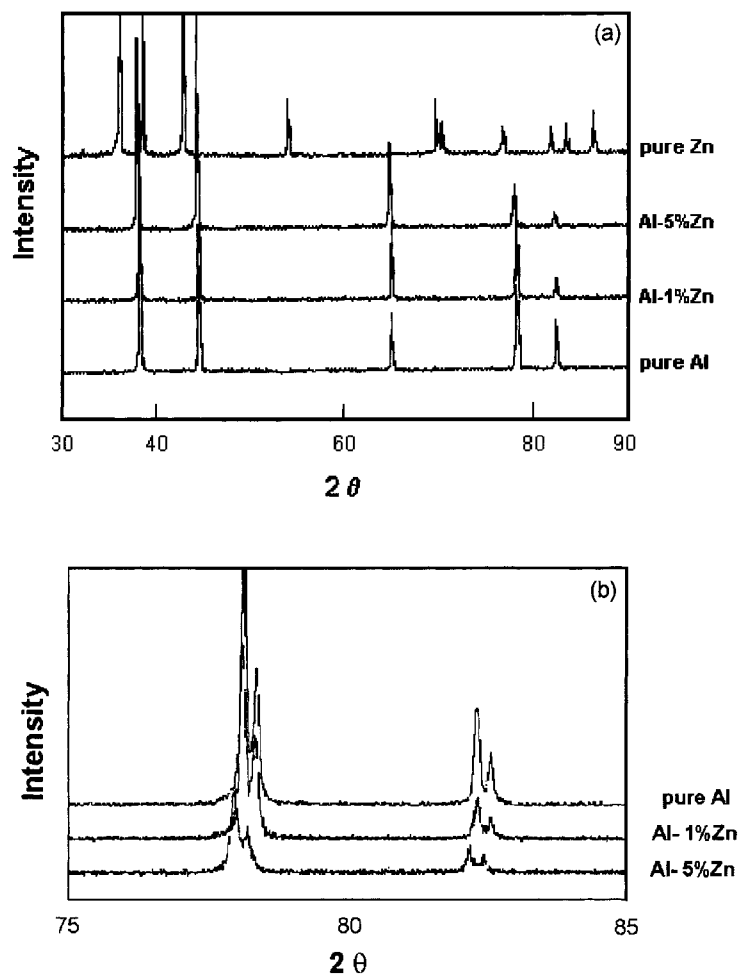

Fig. 7. (a) Results of the diffraction analysis performed on Al$_p$–Zn alloys with low Zn content (1–5 wt %); (b) as (a) but obtained at relatively high diffraction angles.

Table 5. Variation of lattice parameter depending on the Zn content in the alloy

Alloy	Angle, 2θ	$d/\text{Å}$	h k l	Lattice parameter/Å
Al_p	78.12	1.222	3 1 1	4.053
Al_p–1%Zn	78.1	1.223	3 1 1	4.056
Al_p–5%Zn	77.98	1.224	3 1 1	4.062
Al_p	82.32	1.17	2 2 2	4.053
Al_p–1%Zn	82.3	1.1708	2 2 2	4.056
Al_p–5%Zn	82.19	1.1725	2 2 2	4.062

Table 6. Semiquantitative percentage of β phase obtained from the intensity of the characteristic peaks (see Figure 8)

Zn in the alloy /wt %	β phase /%
20	3.08
40	24.83
60	54.62
80	67.43

more concentrated and reactive α phase in those places and inducing operating potentials more negative than the equiaxial structure with the same Zn content.

3.2. *Extended Zn content range (>5 wt % Zn)*

Considering now the X-ray diffraction spectra of those alloys with Zn content greater than 5 wt % (Figure 8), specially the α and β characteristic peaks, an alloy with two phases is confirmed in each case. No characteristic peak shift is detected within the angle phase analysed, but increasing Zn peak intensity is observed, as the Zn content increases. Applying either the direct or absorption differential method [13], a semiquantitative percentage of each phase can be obtained from the intensity of the characteristic peaks (Table 6). This suggests that an increasing β phase area is expected as the Zn content increases.

Figure 9 shows the polarization curves of these alloys obtained after the 30 day galvanostatic run ($i = 1\ \text{mA cm}^{-2}$). The potential rupture is shifted to more negative values at increasing Zn content. Implying that, for example, in the Al–80 wt %Zn alloy the α phase is not being activated and the whole current is sustained by the β phase. Therefore, the attack morphology and, as a consequence, the anode efficiency will depend on the β phase distribution. As an example, Figure 10 shows the variation of the relative element concentration profile within a dendritic growth in the alloy Al–Zn 40 wt %. Clearly Zn rich zones (β phase), following a coring effect, are located in the interdendritic ones.

3.3. *Full Zn content analysis*

Figure 11 shows the operating potentials and the corresponding efficiencies after the 30 day run for the entire Zn content range in the alloy. The efficiency was
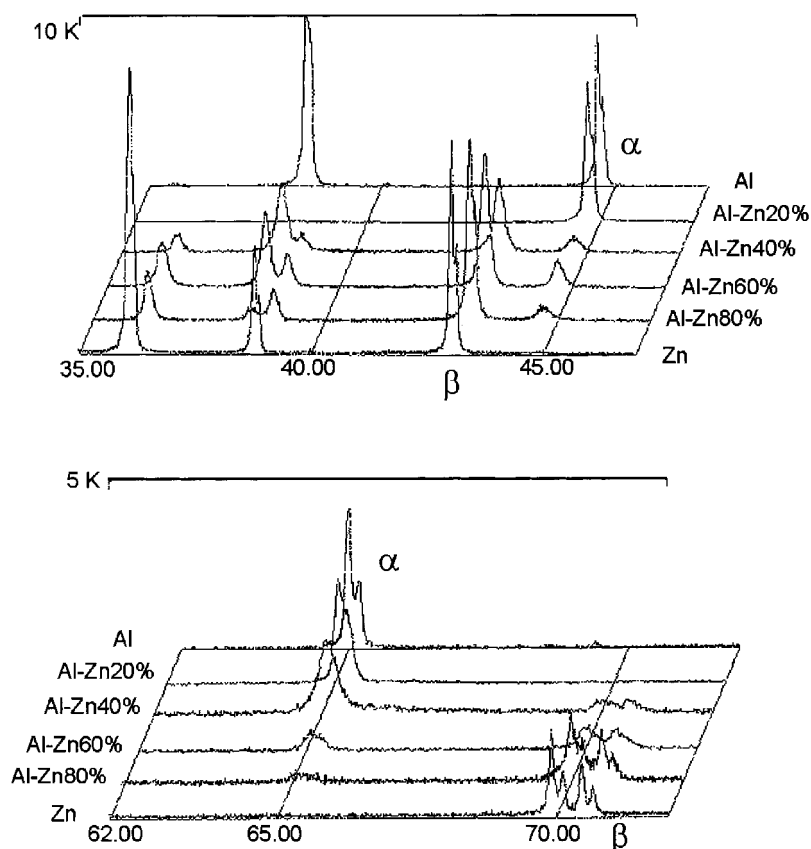

Fig. 8. Results of the diffraction analysis performed on Al_p–Zn alloys with relatively high Zn content (>5–80 wt %).
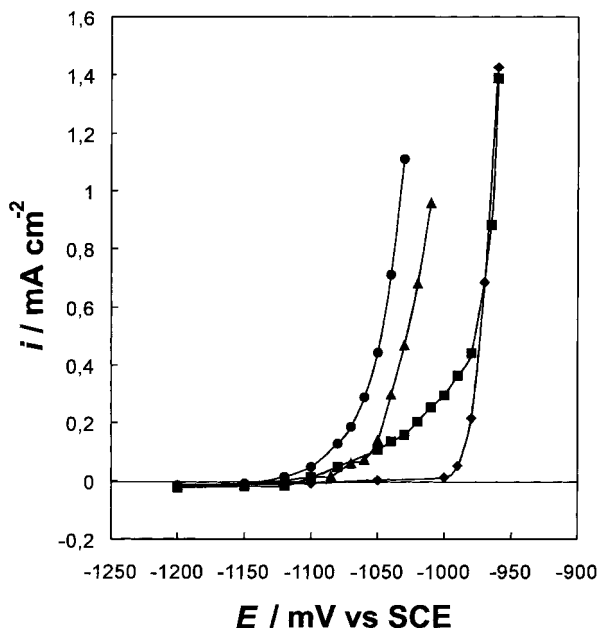
Fig. 9. Galvanostatic polarization curves of Al$_p$–Zn alloys with relatively high Zn content (>5–80 wt %) after the accelerated dissolution test. Solution: 0.5 M NaCl, pH 5. Legend: (◆) Al–20 %Zn, (■) Al–40 %Zn; (▲)Al–60 %Zn; (●) Al–80 %Zn.

calculated considering only the matrix element in the case of α (Al) or β (Zn) single phase alloys, and affected by a proportional factor related to the nominal wt% of the elements present, in the case of alloys with two phases. Only chill and equiaxial structures were considered in this analysis. The columnar structure was disregarded due to the band segregation effect, which produced a heavy mechanical loss, and a very poor anode efficiency. These results can be explained taking into account the electrochemical data obtained and the attack morphology developed after the 30 day run. Once the anode active area reached a steady state value (after pitting propagation) the actual area composition will be proportional to the α/β phase relationship developed by the casting conditions and the nominal composition.

Therefore, the current output will be sustained by these areas, according to their particular E/i relationship. This situation will define the operating potential and the anode efficiency. The β phase defines more active areas, with depolarized kinetics. An increasing amount of β phase shifts the operating potential to more negative values and leads to preferentially dissolution. Depending on its area distribution ($A_\alpha/A_\beta < 1$ or $A_\alpha/A_\beta > 1$)β phase segregation in the grain boundaries or interdendritic zones will favour localized attack and mechanical loss.

Considering the α/β phase relationship obtained from the X-ray diffraction spectra data, five typical cases, depending on the Zn content, are presented to explain alloy electrochemical behaviour:

(a) *1 wt %Zn*: The small amount of Zn is segregated to well localized sites producing deep cavities along grain boundaries or interdendritic zones. Low Zn content increases the grain size. Low efficiencies are expected in the long term because of heavy mechanical loss. The operating potential fluctuates due to undefined α phase distribution, depending on microstructure (chill, columnar or equiaxial).

(b) *5 wt %Zn*: α phase saturation is attained with possible, but undetected, incipient β phase formation. At higher Zn content the grain size is lower. The operating potential is well defined because of the good α phase distribution, and becomes independent of microstructure. Therefore, the best attack distribution gives the best efficiency for this alloy.

(c) *5 wt % < x %Zn ⩽ 40 wt %*: The efficiency is drastically lowered because the area ratio ($A_\alpha/A_\beta > 1$) favours local attack on β phase areas, now formed and segregated, producing a coring effect and giving severe mechanical loss. The operating potential is still sustained by α phase areas and is practically unchanged.

(d) *40 wt % < x %Zn ⩽ 99 wt %*: In these cases $A_\alpha/A_\beta < 1$. The operating potential evolves towards more negative values due to the increasing amount
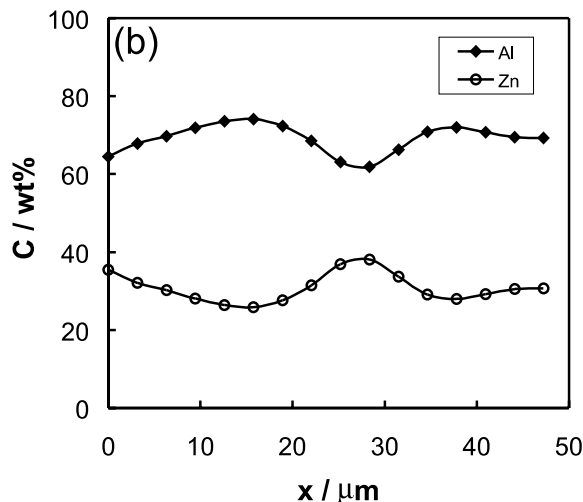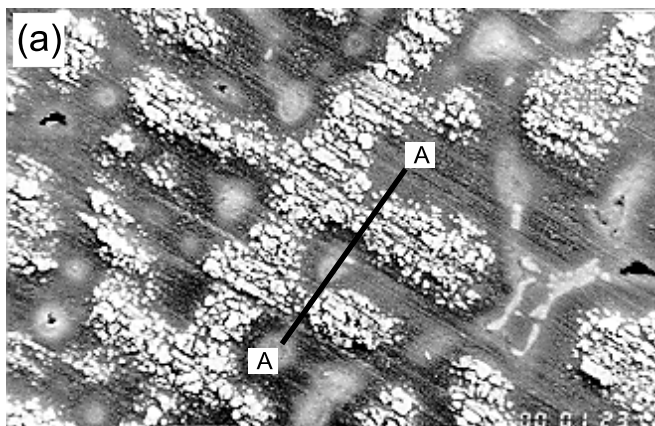

Fig. 10. (a) SEM micrograph of the Al–40 wt %Zn alloy; (b) EDX line profile analysis performed on A–A line. Legend for (b): (◆) Al and (○) Zn.
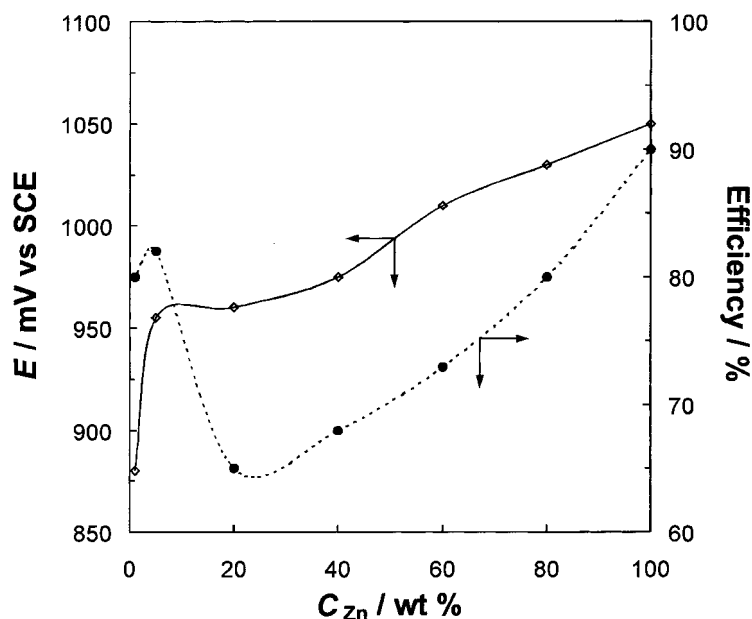
Fig. 11. Efficiencies and operating potentials of the Al–Zn alloys with different Zn content. Legend: (◇) potential and (●) efficiency.

of β phase. The anode efficiency improves because the active areas are now related to the β phase. The α phase areas practically do not work unless strong polarization occurs due to a heavy current output requirement.

(e) *100 wt %Zn*: The highest efficiency for the system is reached (on a pure Zn basis). The most electronegative operating potential is also obtained. This situation appears as the most suitable from the electrochemical point of view (operating potential + efficiency) but from the economic point of view it is useless, due to its poor current capacity compared with that offered by Al and its alloys.

4. Conclusions

(i) According to casting conditions, and for Zn content less than 5 wt %, the interdendritic zones or grain boundaries of Al–x wt %Zn alloys will be the initial sites of attack.

(ii) The operating potential is strongly affected by the solidification macrostructure when the zinc content in the alloy is lower than 3 wt %.

(iii) The solidification macrostructure influences the efficiency values. Depending on casting conditions and zinc content, self corrosion is the principal cause of efficiency loss.

(iv) Casting conditions that produce better alloying element distribution in enriched zones, will promote higher efficiency.

(v) For Zn contents higher than 5 wt %, the operating potential and the anode efficiency will be defined by the α/β phase area relationship. The β phase

defines more active potentials and its segregation, in grain boundary or interdendritic zones, favours localized attack and mechanical loss.

References

1. M.G. Flemings, 'Solidification Processing' (McGraw-Hill, New York, 1974).
2. J.T. Reading and J.J. Newport, *Mater. Protect.* **5** (1966) 15.
3. D.R. Salinas and J.B. Bessone, *Corrosion* **47** (1991) 665.
4. J.B. Bessone, R.A. Suarez Baldo and S.M. de De Micheli, *Corrosion* **37** (1981) 533.
5. J. Morgan, 'Cathodic Protection' (NACE, 1995), chapter 4. p. 113.
6. L.L. Shreir, 'Corrosion', Vol. 2 (Butterworths, London 1978), p. 11–21.
7. P.R. Sperry and M.H. Bankard, Metallographie Techniques for Aluminum Alloys, in 'Metals Handbook', 8th edn., Vol. 8, (ASM, Metals Park, OH, 1973), p. 120.
8. D.T. Hawkins and R. Hultgren, Constitution of Binary Alloys, in 'Metals Handbook', 8th edn., Vol. 8, (ASM, Metals Park, OH, 1973), p. 265.
9. A. Zahra, C.Y. Zahra and R. Ciach, *J. Thermal Anal.* **26** (1983) 303.
10. J.R. Scott and H. Lee Craig, Jr, Proceedings 4th NACE Meeting (1971), p. 179.
11. G. Knörnschild, J. Heldt, H. Mitterbacher and H. Kaesche, *Werkst. Korros.* **46** (1995) 572.
12. I.L. Müller and J.R. Galvele, *Corr. Sci.* **17** (1977) 995.
13. D.H. Hooton and N.E. Giorgetta, *X-Ray Spectrom.* **6** (1977) 2.